LASER INTERFEROMETER GRAVITATIONAL WAVE OBSERVATORY
- LIGO -
CALIFORNIA INSTITUTE OF TECHNOLOGY
MASSACHUSETTS INSTITUTE OF TECHNOLOGY

Technical Note	**LIGO-T1400334–vX**	2014/09/26

Thermal Noise Reduction in Coating-Less Optical Cavities

Sam Moore

California Institute of Technology
LIGO Project, MS 18-34
Pasadena, CA 91125
Phone (626) 395-2129
Fax (626) 304-9834
E-mail: info@ligo.caltech.edu

Massachusetts Institute of Technology
LIGO Project, Room NW22-295
Cambridge, MA 02139
Phone (617) 253-4824
Fax (617) 253-7014
E-mail: info@ligo.mit.edu

LIGO Hanford Observatory
Route 10, Mile Marker 2
Richland, WA 99352
Phone (509) 372-8106
Fax (509) 372-8137
E-mail: info@ligo.caltech.edu

LIGO Livingston Observatory
19100 LIGO Lane
Livingston, LA 70754
Phone (225) 686-3100
Fax (225) 686-7189
E-mail: info@ligo.caltech.edu

http://www.ligo.caltech.edu/

Abstract

Lasers need to have low frequency and phase noise when used in high-precision measurements (such as gravitational wave detection). Advanced LIGO's laser cavities contain coatings that are subject to Brownian noise, which is the dominant noise source in the 40 - 100 Hz regime. Here we test the feasibility of a coating-less optical cavity in reducing the total noise. To achieve such cancellation, we focus on reducing thermal noise, namely thermoelastic (TE) noise (associated with length fluctuations) and thermorefractive (TR) noise (associated with index of refraction fluctuations).

Since TE and TR arise from the same source—thermal fluctuations—we expect correlation between them, allowing for possible cancellation. However, only partial correlation—and hence partial cancellation—was found. The thermal noise reduction was not enough compared to the noise in cavities with reflective coatings. Our optical cavity is a rectangular block, utilizing total internal reflection instead of reflective coatings. A fast method is presented here for thermal noise calculations, which rely on Finite Element Analysis (FEA) software. For thoroughness, the next step is to determine if different geometries allow better cancellation. However, this is not expected, since the laser beam is believed to be too small to notice differences in geometry.

1 Motivation

Laser frequency stabilization is important for use in high-precision measurements (such as gravitational wave detection). The cavity from which the laser originates contains many sources of noise, such as thermal and mechanical fluctuations [1]. To achieve the precision necessary for gravitational wave detection, this project aims to reduce noise in these cavities. Most stabilization cavities contain reflective coatings, which have the problem of high Brownian noise, as shown in figure 1 from Kessler et al [2]. As a result, this project removes the reflective coatings in the resonator and instead uses total internal reflection (TIR).

2 TIR Cavity

A TIR cavity removes all of the multilayer coatings that are usually present. In doing so, losses upon reflection are reduced; as mentioned previously, Brownian noise is prevalent in multilayer coatings. The cavity operates by using total internal reflection (TIR), which requires that $n_2 < n_1$ [3], where n_1 is the index of refraction of the cavity, and n_2 is the index of refraction of the surrounding medium. Furthermore, the angle of incidence θ inside of the medium n_1 must satisfy $\sin\theta > n_2/n_1$ for TIR to occur. This means that the values by which n_1 and n_2 differ depends on the geometry of the cavity. For example, if we describe total internal reflection inside of a square, $\theta = 45°$, so $n_1/n_2 > 1.41$. For a triangle, meanwhile, $n_1/n_2 > 2$.

How does the light first get into and out of the cavity? It "leaks" into the cavity by use of frustrated total internal reflection. As discussed in Schiller et al, another material is placed

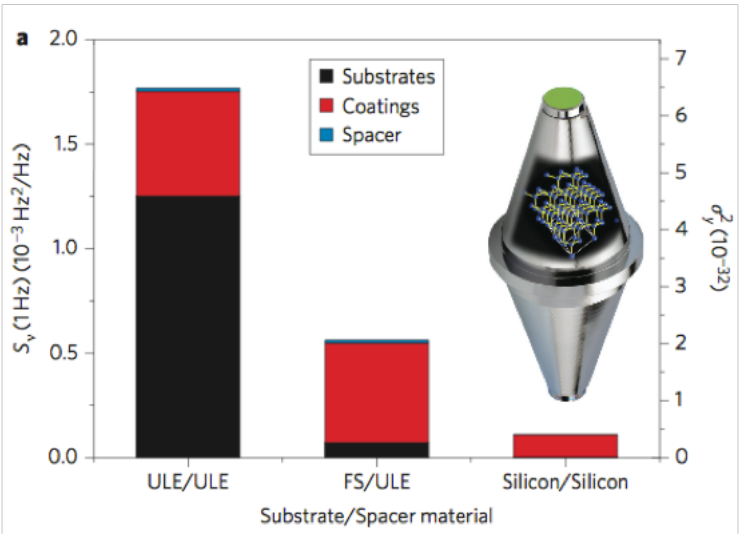

Figure 1: From Kessler et al, the coating Brownian noise is shown in red for various substrate materials in an optical cavity.

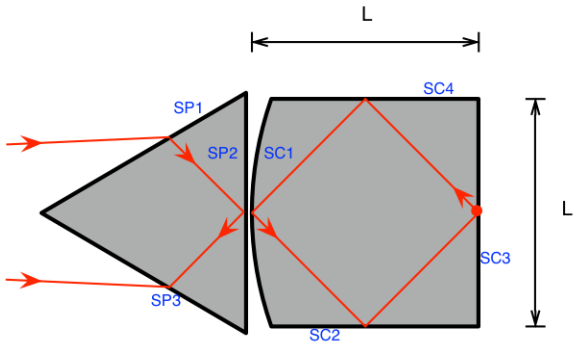

Figure 2: The coating-less total internal reflection (TIR) cavity. A prism and cavity are separated a distance on the order of the wavelength of the laser light. When the light enters the prism, an evanescent part of the light enters the cavity (a process called frustrated total internal reflection).

a distance of order λ (light wavelength) from the cavity. This allows an evanescent wave to travel into and out of the cavity.

3 Thermal Noise

High-precision optical cavities deal with many sources of noise, which is why it is important to have a strong signal. For this report, we focus on the thermal noise: Thermoelastic (TE) noise, and Thermorefractive (TR) noise. The current section discusses how to calculate these forms of thermal noise.

3.1 Fluctuation Dissipation Theorem

The Fluctuation Dissipation theorem (FDT) will be the primary tool used to calculate the thermal noise. The central idea of the FDT is that fluctuations cause dissipation. Hence, if we have low fluctuations, there will also be low dissipation. Notice that this is relating a microscopic property to a macroscopic property. The dissipation (a macroscopic property) is usually the observed property, which means that it can be used to infer the thermal fluctuations. See Callen & Welton [4] for a detailed derivation of the FDT.

Fluctuations are quantified by the power spectral density $S_\xi(\omega)$, which gives the rms value of the random variable ξ, per unit frequency. Assuming that the mean value of ξ is 0, $S_\xi(\omega)$ is a variance density.

3.2 Levin's Approach

Levin's approach utilizes the FDT to calculate thermal noise. The technique works for non-uniform dissipation and an arbitrary laser beam size. To calculate the thermal noise $S_z(f)$ associated with a displacement z at a frequency f, one applies, at time t, an oscillatory generalized force $F_0 \cos(2\pi f t) f(\vec{r})$ to the geometry of interest (the "test mass") [5]. $f(\vec{r})$ indicates the spatial distribution of the applied force beam on the geometry and F_0 is an arbitrary amplitude. In this process, one can calculate W_{diss}, the dissipation associated with the applied force. From the FDT, $S_z(f)$ can then be calculated via

$$S_z(\omega) = \frac{8 k_B T}{\omega^2} \frac{W_{\text{diss}}}{F_0^2} \tag{1}$$

where T is the temperature of the test mass, k_B is Boltzmann's constant, and $\omega = 2\pi f$. Note that the F_0 term is not necessary to calculate because it cancels out with the F_0 in the expression for W_{diss}.

3.3 Brownian Noise

We have previously mentioned Brownian noise when discussing reflective coatings. This is an effect that arises out of Brownian motion, where particles in a fluid are observed to jostle randomly while suspended in a fluid. Brownian noise manifests itself as slight, fluctuating distortions in the shape of the cavity. Brownian noise can occur in an optical cavity's reflectors, and is especially prevalent in multilayer mirror coatings (see Kessler et al. [2] for Brownian noise in different materials). The purpose of this report is to remove these coatings in an attempt to reduce Brownian noise.

3.4 Thermorefractive Noise

Thermorefractive (TR) noise is caused by fluctuations in the index of refraction of the cavity due to stochastic fluctuations in the material's temperature. The result of these fluctuations is that radiation in the cavity develops random fluctuations in its phase. The thermorefractive index $\beta \equiv \frac{\partial n}{\partial T}$ characterizes this TR noise (where n is the index of refraction). For

Thermorefractive noise, the generalized force of the Levin Approach has the form of an oscillatory heat source [7]:

$$q(\vec{r},t) = T(\vec{r},t)F_0\cos(2\pi ft)f(\vec{r}) \tag{2}$$

where $T(\vec{r},t)$ describes the temperature distribution at a point $\vec{r}$ and time t. $f(\vec{r})$ describes the shape of the laser beam as it propagates through the cavity. Given the heat source in equation 2, one can solve for the temperature distribution via the heat equation:

$$C_p\frac{\partial T}{\partial t} - \kappa\nabla^2 T = \dot{q}(\vec{r},t), \tag{3}$$

where C_p is the heat capacity per volume at constant pressure and κ is the thermal conductivity. Now, temperature *gradients* are the true quantities of interest because they cause heat flux—and therefore energy dissipation—in the test mass. The dissipation is related to the temperature gradient via

$$W_{\text{diss}} = \frac{1}{2T_0}\int_V \kappa|\nabla T|^2\, dV \tag{4}$$

where κ is the thermal conductivity and T_0 is a homogeneous reference temperature of the test mass. From this, one can use the FDT (eq. 1) to calculate the thermal noise.

Solving the time-dependent heat equation can be computationally expensive, since one must deal with complicated transients and average over them when calculating W_{diss}. To avoid such time-consuming procedures, we assume a steady-state temperature $T(\vec{r},t) = T(\vec{r})e^{i\omega t}$, given a heat injection $q(\vec{r},t) = q(\vec{r})e^{i\omega t}$. This yields a frequency-domain differential equation of the form

$$i\omega C_p T(\vec{r}) - \kappa\nabla^2 T(\vec{r}) = i\omega q(\vec{r}) \tag{5}$$

With this time-saving method, one can use eq. 4 without dealing with transient temperature distributions.

3.5 Thermoelastic Noise

Another source of thermo-optic noise is thermoelastic (TE) noise, thermal length expansions due to stochastic temperature fluctuations. These thermal fluctuations cause the cavity to create small, fluctuating deformations throughout its surface. These geometry changes then cause laser frequency noise. TE noise is characterized by the thermal expansion coefficient $\alpha \equiv \frac{1}{L}(\frac{\partial L}{\partial T})$, where L is the linear dimension of the cavity.

Following the Levin approach, one applies a surface stress (units of pressure) $F_0 f(\vec{r})e^{i\omega t}$ incident normal to the cavity. With these boundary conditions, one calculates the elastic displacement field $\vec{u}$ of the cavity by solving

$$(1-2\sigma)\nabla^2\vec{u} + \nabla(\nabla\cdot\vec{u}) = 0, \tag{6}$$

where σ is the Poisson's ratio of the material in question (see [6] for more about elasticity). The elastic displacement will cause temperature changes in the material, proportional to the

material's coefficient of linear thermal expansion α. These temperature changes cause a heat to flow in the material:

$$q(\vec{r}) = -\frac{\alpha E T_0}{1-2\sigma}\nabla \cdot \vec{u} \tag{7}$$

With the heat injection from the elastic displacement, one then solves the heat equation in eq. 5, assuming steady-state, harmonic temperature and displacement field oscillations. From here, one applies eq. 4 and 1 to calculate the TE noise.

3.6 Thermo-optic Noise

TE and TR noise can be combined together, which is the aim of this project. Evans et. al [**?**] showed that in a cavity with multilayer coatings, the TE and TR mechanisms have a negative relative sign in the overall thermal noise ("thermo-optic" noise) spectrum, leading to possible thermal noise cancellation. However, this relative negative sign does not occur with coating-less cavities. As a result, we seek materials whose parameters α and β *themselves* have a relative sign difference [1].

To get an intuition for this cancellation, note that the optical path length $OPL = nL$ determines the phase of the laser beam as it travels through the cavity. That means the noise fluctuations in the phase are given by fluctuations in the optical path length:

$$d(OPL) = (\beta + n\alpha)dT, \tag{8}$$

assuming, for simplicity, a uniform temperature distribution in the cavity. This says that we can eliminate thermal noise in the cavity if we choose α to be equal and opposite to β/n.

In this simplified case, TE and TR noise are 100 percent correlated, since both arise from the same temperature fluctuations. In reality, however, the temperature distribution is not uniform, as figure 3 suggests. And since TR probes an exponentially small region around a propagating laser beam, while TE probes the surface of the cavity, we may only achieve partial correlation at best.

Let's look at the general, partially correlated case. Note that S_{TO} is the variance of a sum of two random variables, associated with TE and TR noise respectively. As a result,

$$S_{TO} = S_{TE} + S_{TR} + 2R\sqrt{S_{TE}S_{TR}}, \tag{9}$$

where R is the correlation coefficient between the TR and TE noise. We can get perfect cancellation if $R = -1$ (perfect anti-correlation) and $S_{TE} = S_{TR}$. We expect to achieve this anti-correlation by choosing α and β to have an opposite sign.

4 Finite Element Analysis

COMSOL and MATLAB have been used to simulate the sources of noise. The COMSOL model utilizes Finite element analysis and the Fluctuation Dissipation theorem.

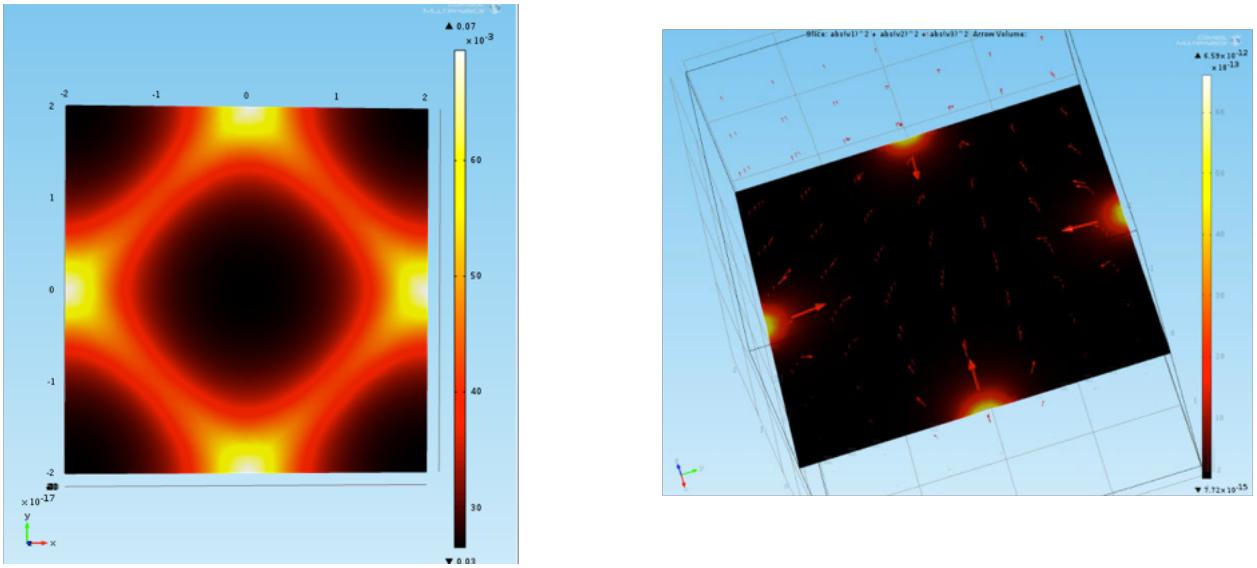

Figure 3: Temperature distributions in the TIR cavity. Left: the temperature distribution from TR calculations, which is confined to the propagating laser beam. Right: the temperature distribution from TE calculations (with the displacement vector field), which remains confined to the surface. Since the temperature distributions are different, we expect only partial correlation.

4.1 Test Cases

Here, we check the COMSOL model for TR noise in cylindrical test masses, as presented in Heinert et al [7]. The aim is to calculate the TR noise in a cylinder subject to adiabatic boundary conditions ($\nabla T = 0$ at the boundary). Heinert et al. derives a plot for this TR noise $\sqrt{S_z(f)}$, where f is the frequency of a heat injection, following Levin's approach. The heat injection is assumed to be of the form of equation 2. If one further assumes small temperature fluctuations, $T(\vec{r}, t)$ in equation 2 can be taken as a constant ambient temperature T_0.

We assume the laser is a Gaussian beam. Hence, for the cylindrical test mass, we have that $f(\vec{r}) = \frac{\beta}{\pi r_0^2} e^{-r^2/r_0^2}$, where r is the distance from the center of the cylinder, and r_0 is the beam radius. We can therefore write $q(\vec{r}) = Ae^{-r^2/r_0^2}$, where $A \equiv \beta T_0 F_0/(\pi r_0^2)$. Once COMSOL calculates the temperature profile, the dissipation is calculated via equation 4, and the TR noise is calculated via equation 1. Heinert's paper derives a TR displacement noise expression of

$$S_z(\omega) = \frac{16}{\pi} k_B T_0^2 \frac{H\kappa\beta^2}{r_0^4 C_p^2} \times \sum_{n=1}^{\infty} \frac{a_n^2}{[J_0(a_n)]^2} \frac{K_n^2}{\omega^2 + \frac{\kappa^2 a_n^4}{C_p^2 R^4}} \tag{10}$$

where $J_0(x)$ is the zeroth order bessel function of the first kind, R is the radius of the cylinder, H is the height, a_n is a zero of $J_1(x)$, and

$$K_n = \int_0^1 J_0(a_n \rho) e^{-((R/r_0)\rho)^2} \rho \, d\rho \tag{11}$$

The following noise plot in figure 4 was obtained for a silicon test mass at $T_0 = 10$ K. The solid line represents the analytical calculation, eq. 10, while the dots represent COMSOL's calculations. Two COMSOL models were used: a 1D axisymmetric model, and a full-scale 3D cylindrical model. Both use the fast steady-state frequency-domain approach for the heat equation (eq. 5).

In figure 4, as well as many other of the upcoming plots, we find that the noise levels off for low frequency. The intuition for this effect is that at low frequencies, the temperature is able to equilibrate throughout the body; this uniform temperature implies that there are no temperature gradients, and hence no heat flow.

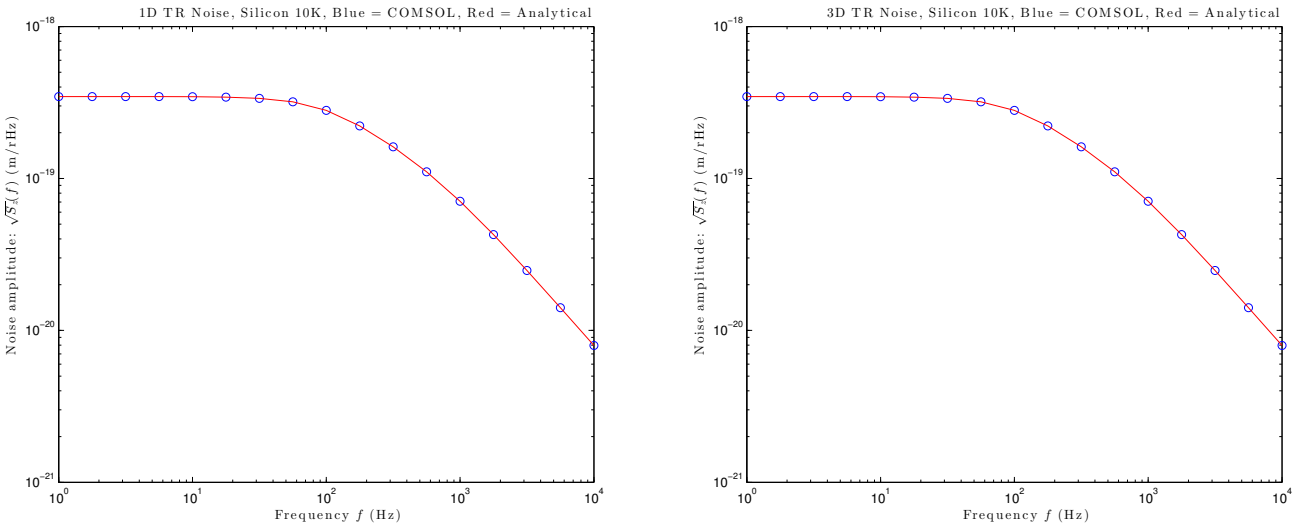

Figure 4: Displacement TR noise as a function of frequency f for silicon at 10 K. The verification is shown for two different types of models in COMSOL. The 3D model (right) is the most general model, and it still runs much faster than the previous time-dependent model.

Figure 4 shows that a 1D axisymmetric model (left) and a full 3D model (right) in COMSOL both yield agreement with the red analytical curve (eq. 10). It should also be emphasized that the steady-state temperature approach in eq. 5 allowed these plots to be generated much faster than before.

4.2 TIR Cavity

In the previous section, we found that the frequency domain, steady-state approach to thermal noise calculations gives accurate results faster than the usual time-dependent approach. We therefore use the same method for thermal noise in the TIR cavity. We assume that the geometry in this case is a rectangular slab of width, length, and height W, L and H, respectively. A laser beam is injected through the center of the slab. That laser, undergoing total internal reflection, is assumed to not lose energy and that it reflects off of the center of the cavity walls. With this setup, the goal is to calculate the overall thermo-optic noise.

We assume, as a first approximation, that the laser consists of four gaussian beams of the

form $e^{-(z^2+x'^2)/r_0^2}$, where x' denotes the horizontal distance from the beam's propagation axis, and z denotes the height. Interference effects at the reflection points are ignored, as are any waists associated with the laser. For TR noise, then, we find that

$$\begin{aligned} q(\vec{r}) = Ae^{-z^2/r_0^2}[&\exp[-(x\sin\theta-(y+L/2)\cos\theta)^2/r_0^2] \\ &+\exp[-((x-W/2)\sin\theta+y\cos\theta)^2/r_0^2]+\exp[-((x+W/2)\sin\theta-y\cos\theta)^2/r_0^2] \\ &+\exp[-(x\sin\theta+(y+L/2)\cos\theta)^2/r_0^2]] \end{aligned} \tag{12}$$

is the heat injection that takes the form of the laser, where $\theta = \tan^{-1}(L/W)$. Also, recall that $A \equiv \beta T_0 F_0/(\pi r_0^2)$.

To calculate the thermal noise, COMSOL must solve equation 5 with this new heat injection. Adiabatic boundary conditions are assumed. One important source of error is in the meshing for this rectangular TIR cavity. We have created different meshing methods, from a uniform, 'extra fine', mesh to finely-meshed cylinders in the shape of the laser beam, surrounded by a coarser mesh. Some different meshings of the TIR cavity are shown in figure 5. While a uniform mesh may not give the most accurate result, it was chosen because other meshings required too much memory for COMSOL to run the simulation.

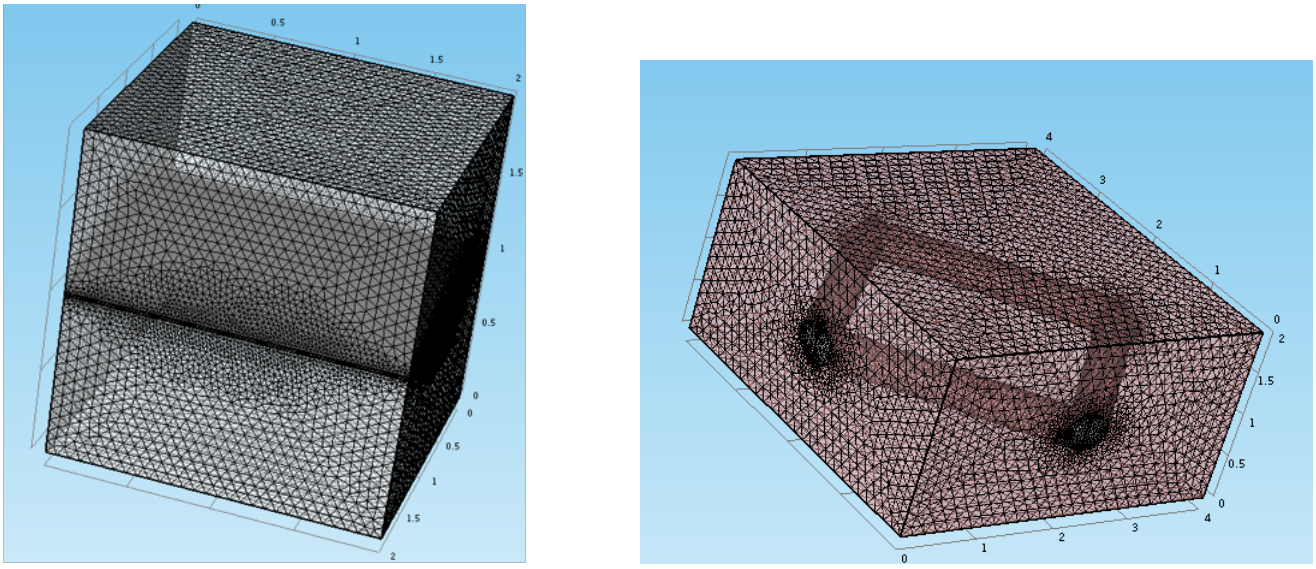

Figure 5: Screenshot from COMSOL, showing a 'sandwich' meshing (left) and a cylinder meshing (right). For the sake of adequate memory allocation, a uniform mesh turned out to be the feasible option.

It is helpful to have an analytical solution to compare to COMSOL. Consider a rectangular slab whose origin is at the center. The x, y, and z lengths are W, L, and H, respectively. For adiabatic boundary conditions, we therefore require

$$(\nabla T)_x|_{x=\pm\frac{W}{2}} = (\nabla T)_y|_{y=\pm\frac{L}{2}} = (\nabla T)_z|_{z=\pm\frac{H}{2}} = 0 \tag{13}$$

for the temperature field, which satisfies the steady-state heat equation (eq. 5) where q is the heat injection. In the absence of a heat injection, we know that T can be written as a

Fourier series. Hence, we seek a solution of the form

$$T(\vec{r}) = \sum_{lmn} a_{lmn} \cos(r_l x) \cos(r_m y) \cos(r_n z) + b_{lmn} \sin(s_l x) \sin(s_m y) \sin(s_n z) \tag{14}$$

We will use the Fourier expansion of $q(\vec{r})$ to determine a_{lmm} and b_{lmm}. The z-dependence of q should be emphasized here: a Gaussian e^{-z^2/r_0^2}, where r_0 is the beam radius. This is an even function, which means that we only need to keep the cosine terms in the expansion for $T(\vec{r})$. In other words, $b_{lmn} = 0$. Since

$$\begin{aligned}\nabla T = -\sum_{lmn} a_{lmn} [&r_l \sin(r_l x) \cos(r_m y) \cos(r_n z), \\ &r_m \cos(r_l x) \sin(r_m y) \cos(r_n z), r_n \cos(r_l x) \cos(r_m x) \sin(r_n x)],\end{aligned} \tag{15}$$

the boundary conditions (eqs. 13) give us

$$\frac{r_l W}{2} = l\pi, \quad \frac{r_m L}{2} = m\pi, \quad \frac{r_n H}{2} = n\pi \tag{16}$$

where l, m, n are integers. If we make them even integers, then we can write

$$T(\vec{r}) = \sum_{\text{even}} a_{lmn} \cos\left(\frac{l\pi x}{W}\right) \cos\left(\frac{m\pi y}{L}\right) \cos\left(\frac{n\pi z}{H}\right) \tag{17}$$

Our goal is to calculate to $S_z(\omega)$, which means we need to calculate the dissipation in eq. 4. Using the orthogonality relation

$$\int_{-W/2}^{W/2} \cos\left(\frac{l\pi x}{W}\right) \cos\left(\frac{l'\pi x}{W}\right) dx = \frac{W}{2} \delta_{ll'} \tag{18}$$

we then obtain

$$W_{\text{diss}} = \frac{\kappa \pi^2 V}{16 T_0} \sum_{\text{even}} |a_{lmn}|^2 \left(\frac{l^2}{W^2} + \frac{m^2}{L^2} + \frac{n^2}{H^2}\right) \tag{19}$$

where $V = WLH$. This gives, using eq. 1,

$$S_z(\omega) = \frac{8 k_B T_0}{\omega^2} \frac{W_{\text{diss}}}{F_0^2} = \frac{\kappa k_B \pi^2 V}{2\omega^2 F_0^2} \sum_{\text{even}} |a_{lmn}|^2 \left(\frac{l^2}{W^2} + \frac{m^2}{L^2} + \frac{n^2}{H^2}\right) \tag{20}$$

Now we wish to determine a_{lmn}. To do this, we plug $T(\vec{r})$ into equation 5 and expand $q(\vec{r})$ as

$$q(\vec{r}) = \sum_{\text{even}} c_{lmn} \cos\left(\frac{l\pi x}{W}\right) \cos\left(\frac{m\pi y}{L}\right) \cos\left(\frac{n\pi z}{H}\right), \tag{21}$$

which means that

$$c_{lmn} = \frac{8}{V} \int q(\vec{r}) \cos\left(\frac{l\pi x}{W}\right) \cos\left(\frac{m\pi y}{L}\right) \cos\left(\frac{n\pi z}{H}\right) dV \tag{22}$$

Equation 5 then gives

$$i\omega c_{lmn} = a_{lmn} \left[i\omega C_p + \kappa \left(\frac{l^2\pi^2}{W^2} + \frac{m^2\pi^2}{L^2} + \frac{n^2\pi^2}{H^2}\right)\right] \tag{23}$$

or,

$$|a_{lmn}|^2 = \frac{c_{lmn}^2}{C_p^2 + \frac{\kappa^2\pi^4}{\omega^2}\left(\frac{l^2}{W^2} + \frac{m^2}{L^2} + \frac{n^2}{H^2}\right)^2} \tag{24}$$

Plugging this into equation 20, we find that

$$S_z(\omega) = \frac{\kappa k_B \pi^2 V}{2F_0^2} \sum_{\text{even}} \frac{|c_{lmn}|^2}{C_p^2\omega^2\left(\frac{l^2}{W^2} + \frac{m^2}{L^2} + \frac{n^2}{H^2}\right)^{-1} + \kappa^2\pi^4\left(\frac{l^2}{W^2} + \frac{m^2}{L^2} + \frac{n^2}{H^2}\right)} \tag{25}$$

For convenience, let $d_{lmn} = c_{lmn}/A$. Then

$$S_z(\omega) = \frac{\kappa k_B T_0^2 \beta^2 V}{2r_0^4} \sum_{\text{even}} \frac{|d_{lmn}|^2}{C_p^2\omega^2\left(\frac{l^2}{W^2} + \frac{m^2}{L^2} + \frac{n^2}{H^2}\right)^{-1} + \kappa^2\pi^4\left(\frac{l^2}{W^2} + \frac{m^2}{L^2} + \frac{n^2}{H^2}\right)} \tag{26}$$

We considered the following parameters: $L = W = H = 4$ cm, $T = 120$ K, $r_0 = 2$ mm, $\beta = 8.7 \times 10^{-5}$ K^{-1}, $C_p/\rho = 328$ J/kg/K, $\rho = 2331$ kg/m^3, $\alpha = -0.057 \times 10^{-6}$ K^{-1} and $\kappa = 615$ W/m/K. Given these parameters, the Fourier coefficients were plotted to determine the proper cutoff indices in the triple sum of equation 26 . Note that the heat injection can be written in the form $q(\vec{r}) = q(z)q(x, y)$. This separation of variables means that we can write $d_{lmn} = d_n d_{lm}$, where d_n is the z-component of the Fourier coefficient, and d_{lm} is the xy component of the Fourier series. These coefficients are shown in figure 6. They suggest that we can truncate the series at $n = 30$ and $l = m = 20$.

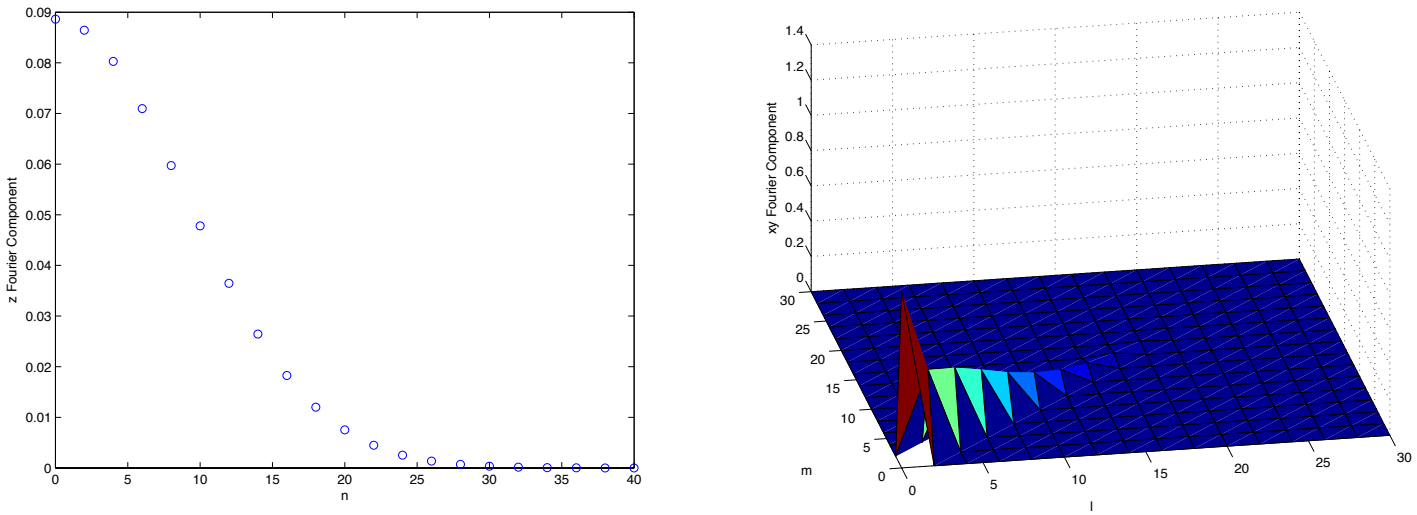

Figure 6: The z-component should go out to about 30 terms, while the xy components should go out to about 20 terms. Moreover, the diagonal $m = l$ only contributes to the Fourier series, allowing us to neglect many terms.

By contrast, a beam size of $r_0 = 0.1$ mm requires many more terms, as indicated in figure 7. This makes sense for the following the reason. The Fourier series terms have an effective wavelength which go as L/m. For an accurate solution, we need to resolve down to the smallest length scales, which means that $m_{\max}$ satisfies $L/m_{\max} \sim r_0$. Hence, if $L \sim 10^{-2}$ m and $r_0 \sim 10^{-4}$ m, then $m_{\max} \sim 10^2$.

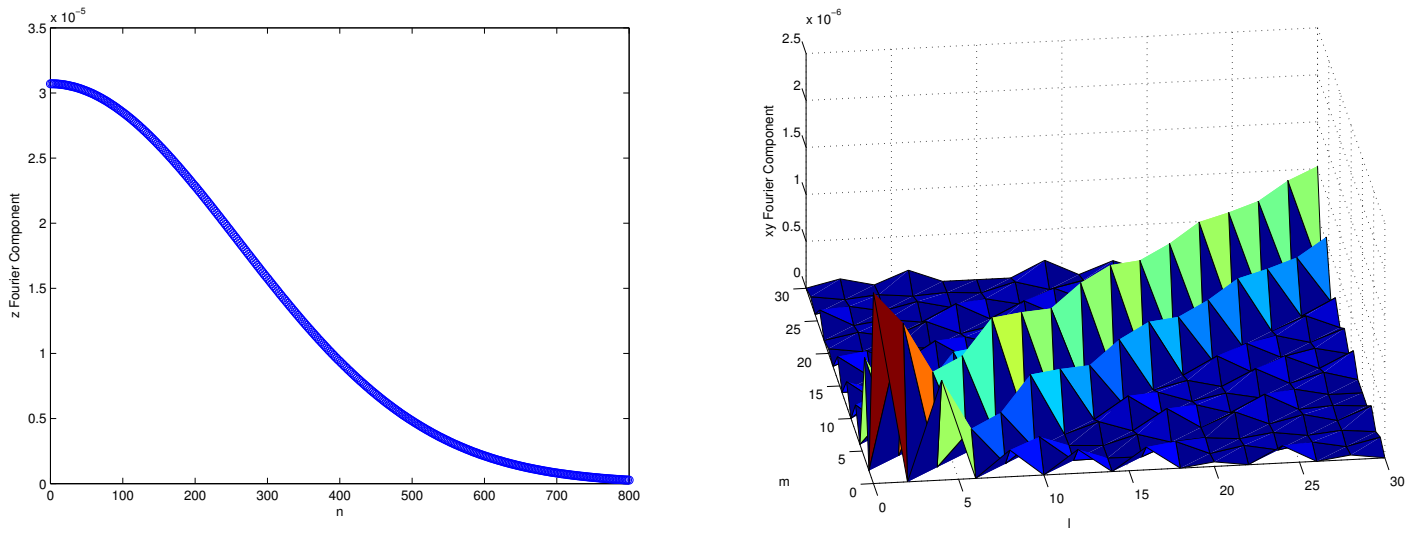

Figure 7: A smaller beam size requires more terms before the Fourier Series converges.

Taking these plots into account, we can have more confidence in the accuracy of the analytical Fourier Series solution. The analytical solution in equation 26 therefore gives a tool for assessing the accuracy of the numerical solution. Furthermore, there is a separate analytical solution given in appendix E of Braginsky et al. 2004 [8]:

$$S_z(\omega) = \frac{k_B T^2}{\pi} \frac{2\beta^2}{\kappa} \sqrt{W^2 + L^2} \int_0^\infty \frac{x e^{-x}\, dx}{\left(\frac{\omega r_0^2 C_p}{2\kappa}\right)^2 + x^2} \tag{27}$$

These two analytical solutions allow us to assess the accuracy of the meshing. At the moment, it appears that a uniform meshing is giving the closest agreement to the analytical model. The left plot of figure 8 shows the agreement between the analytical and numerical models. A reference line is shown, taking a high frequency limit in equation 27. The differences between the analytical and numerical solutions are likely attributed to meshing inaccuracies. In COMSOL, the mesh size runs from 0.008 to 0.11 cm. Meanwhile, the smallest length scale is the thermal wavelength $r_{\text{th}} = \sqrt{\kappa/(C_p \omega)} \sim 10^{-2}$ cm for a frequency of 10^4 Hz. The mesh size is often larger than this, indicating that meshing could be an issue at high frequencies. Furthermore, a beam size of 1 mm may also yield some meshing difficulties, since that is slightly below the maximum mesh size.

The plot on the right of 8 shows the comparison between TR frequency noise and the best coating cavity frequency noise [2]. TR displacement noise was converted to frequency noise S_f via

$$S_f(\omega) = \frac{S_z(\omega)}{L_{\text{roundtrip}}^2} \left(\frac{c}{\lambda}\right)^2 \tag{28}$$

where $L_{\text{roundtrip}} = 2\sqrt{W^2 + L^2}$ is the roundtrip path length of the laser, c is the speed of light, and $\lambda = 1550$ nm is the wavelength of the laser light. An optimal TIR cavity should beat the coating frequency noise. This, however, does not happen for the TR noise. From

here, the hope is to get the TO noise curve below the coating cavity curve by achieving cancellation.

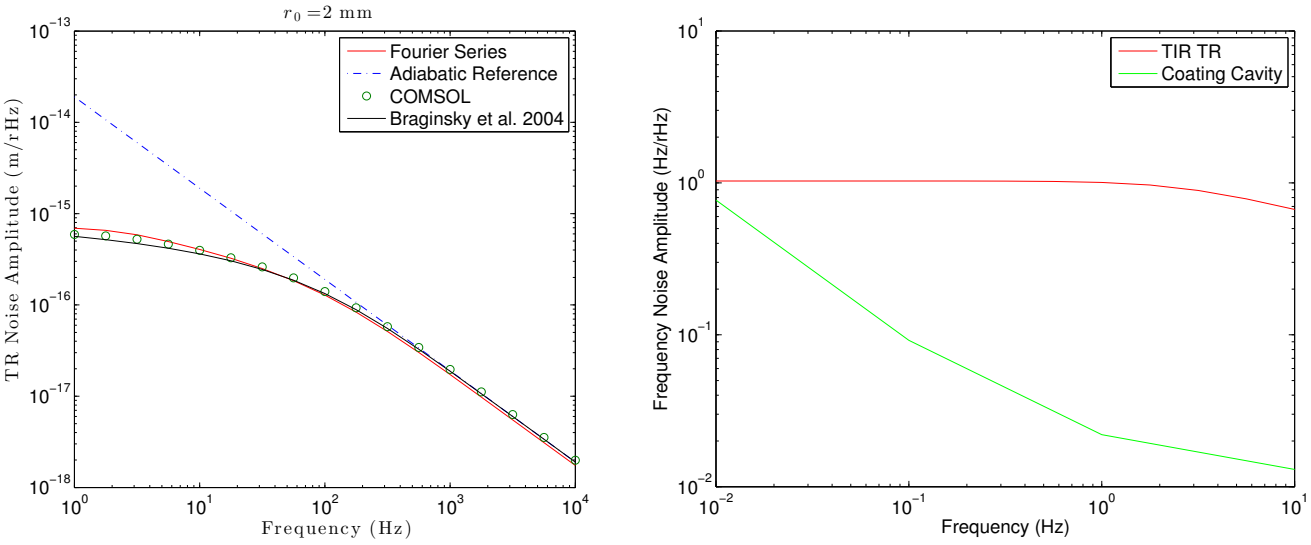

Figure 8: The COMSOL solution for $\sqrt{S_z(f)}$ is compared with the Braginsky and Fourier series solutions. The agreement is better for a larger beam radius such as $r_0 = 2$ mm, which may be attributed to better mesh resolution and faster Fourier series convergence. A uniform 'finer' mesh was used in COMSOL, giving the best agreement among the other sandwich and cylinder meshing ideas. This TR noise is compared with the best coating cavity noise, which turns out to be much smaller.

Hence, the next step in the TIR thermal noise calculation is to calculate the TE noise. We follow the method outlined in section 3.5 for calculating TE noise. For the TIR cavity, the applied strain is $F_0 e^{-r^2/r_0^2}/(\pi r_0^2)$ (removing the oscillatory term for the steady-state approach), directed normally incident upon the faces of the cavity. The elastic displacement field is shown on the right of figure 9. If we can get TE to be on a similar level as TR, it becomes possible to obtain cancellation. Unfortunately, figure 9 shows that the TE and TR noise are on vastly different orders of magnitudes.

To account for the different TE noise value, α was increased to -1.31×10^{-4} K^{-1}, an artificial value used to make TE and TR noise on similar magnitudes. With this new value for α, TO noise was calculated in COMSOL. The TO noise calculation requires solving both the elastic displacement field equations (as in equation 6) and the heat equation. The combined heat injection is $q_{TE}(\vec{r}) + q_{TR}(\vec{r})$, where q_{TR} is the thermorefractive heat injection from the laser beam (eq. 12) and q_{TE} is the thermoelastic heat injection (eq. 7). With the subsequent temperature distribution, one then calculates W_{diss} as usual, leading to a value for the thermo-optic noise $S_{TO}(\omega)$. And with values for S_{TO}, S_{TE}, and S_{TR}, equation 9 was used to calculate the correlation coefficient between TE and TR noise. Figure 10 shows that the TE and TR noise have partial correlation (magnitude less than 1), but not enough to completely cancel TO noise. Moreover, the cancellation is still not enough for the frequency noise to become smaller than the current best reflective cavities as presented in Kessler et al.

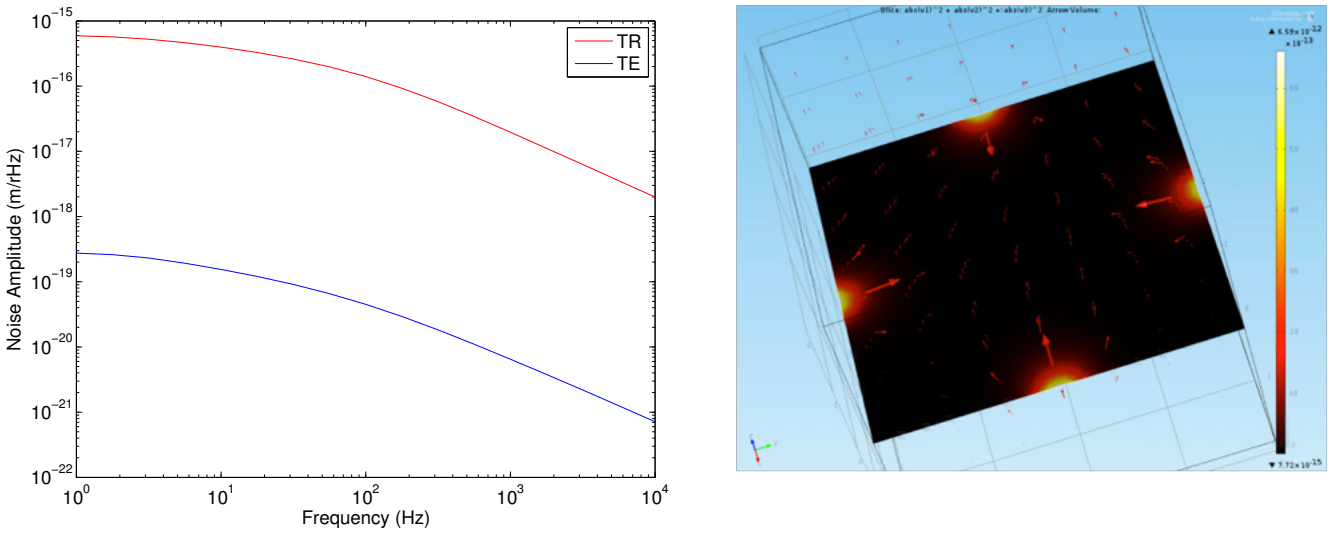

Figure 9: TE calculations. Left: The TE noise is much lower than TR for the current values of α and β. Cancellation will not be possible. Right: The TE noise calculation requires solving for the elastic displacement field, which was calculated in COMSOL.

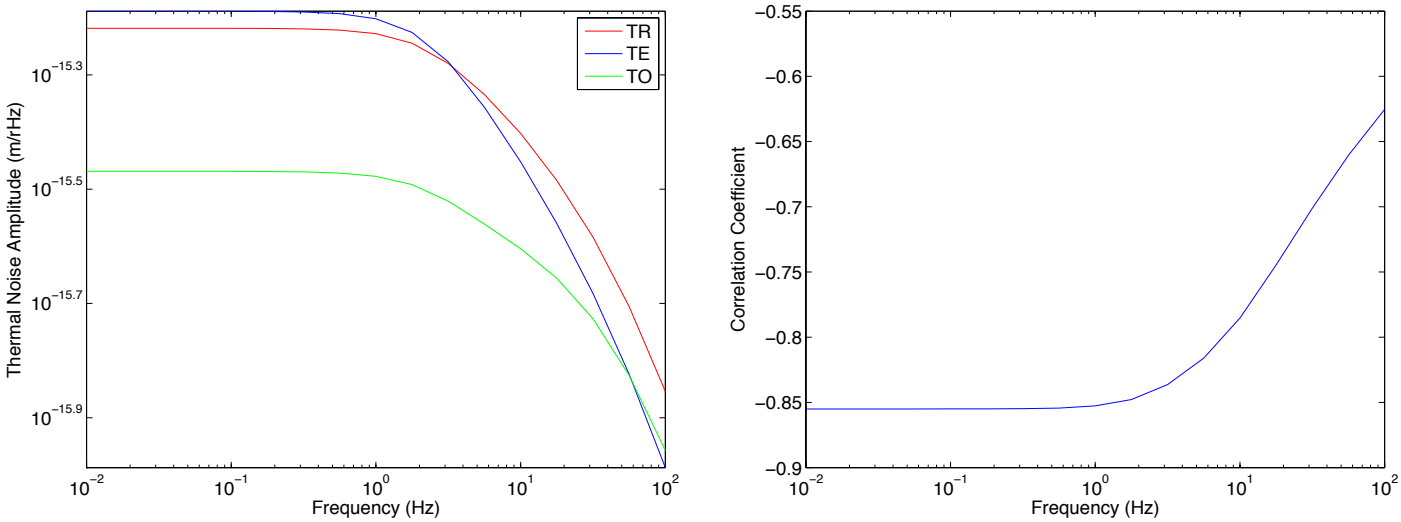

Figure 10: TO noise is calculated here (shown in green on the left plot). Notice that the TO curve is lower than the individual TE and TR curves, which suggests partial cancellation. Indeed, the plot on the right shows that we have a negative correlation coefficient that is not equal to -1. α was scaled to -1.31×10^{-4} to put TE noise on a similar order of magnitude as TR. A 'fine' mesh was used in COMSOL.

5 Conclusion

The TO noise shown in figure 10 indicates that the thermal noise is only partly correlated, leading to partial correlation. This partial correlation may be attributed to the fact that TR noise only arises from a small region around the reflection face of the laser beam, while TE

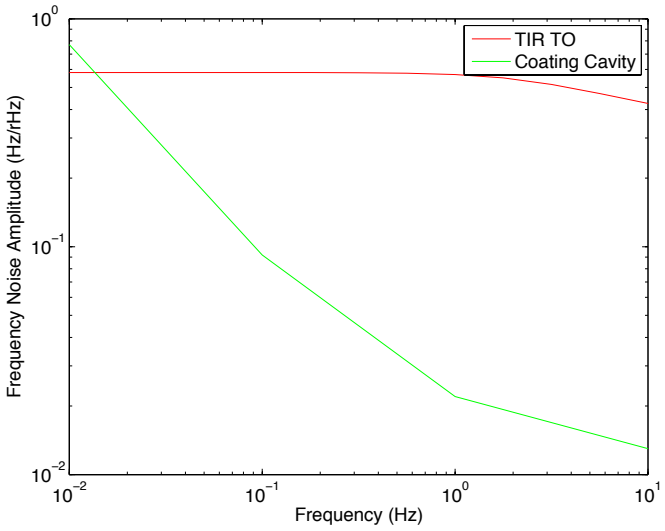

Figure 11: The TO noise is usually orders of magnitude larger than the coating cavity noise. Currently, the TIR cavity has too much noise to be used as a substitute.

noise arises from the entire bulk.

The overall noise in our theoretical optical cavity is too large compared to the current best optical cavities with coatings. Before giving up on this cavity, we can explore whether changes in the geometry of the TIR cavity would lead to better results. We could also do an optimization to get TE and TR closer together.

Appendix: COMSOL Inputs

In this paper, the two partial differential equations being dealt with are

$$i\omega C_p T(\vec{r}) - \kappa \nabla^2 T(\vec{r}) = i\omega q(\vec{r}) \tag{29}$$

and

$$(1-2\sigma)\nabla^2 \vec{u} + \nabla(\nabla \cdot \vec{u}) = 0, \tag{30}$$

To solve this in COMSOL, a stationary solver is used with the coefficient form differential equation module. The equation that COMSOL solves has the form

$$e_a \frac{\partial^2 u}{\partial t^2} + d_a \frac{\partial u}{\partial t} + \nabla \cdot (-c\nabla u - \vec{\alpha} u + \vec{\gamma}) + \vec{\beta} \cdot \nabla u + au = f \tag{31}$$

It should be emphasized that the operator ∇ in this module is only correct for Cartesian coordinates. For a general coordinate system ξ_1, ξ_2, ξ_3, COMSOL assumes $\nabla = (\frac{\partial}{\partial \xi_1}, \frac{\partial}{\partial \xi_2}, \frac{\partial}{\partial \xi_3})$, which is not true in general.

Assuming Cartesian coordinates, we see that our choice of coefficients for 29 is $e_a = d_a = \vec{\gamma} = \vec{\beta} = 0$, $a = i\omega C_p$, $c = \kappa$, and $f = i\omega q(\vec{r})$, where $q(\vec{r})$ is either the TR, TE, or TO

heat injection. For this equation, the 'zero flux' condition in COMSOL is used to implement adiabatic boundary conditions.

Now, 30 requires three Coefficient form modules to be used at once; this is a vector equation whose individual components are coupled. To see how this works, let's look at the u_x component of the equation. In this case, we can write

$$-(1-2\sigma)\left(\frac{\partial^2 u_x}{\partial x^2}+\frac{\partial^2 u_x}{\partial y^2}+\frac{\partial^2 u_x}{\partial z^2}\right)=\frac{\partial^2 u_x}{\partial x^2}+\frac{\partial^2 u_y}{\partial x \partial y}+\frac{\partial^2 u_z}{\partial x \partial z} \tag{32}$$

In this case, we set $c = 1-2\sigma$, $f = \frac{\partial^2 u_x}{\partial x^2}+\frac{\partial^2 u_y}{\partial x \partial y}+\frac{\partial^2 u_z}{\partial x \partial z}$, and zero for all the other coefficients. The oscillating stress is implemented as a Flux/Source boundary condition. Recall that these stresses are directed inward on all sides of the x and y faces. The sign of the flux depends on its direction, which is either positive or negative. For the u_x component, I have a flux of $F_0 e^{-(y^2+z^2)/r_0^2}/(\pi r_0^2)$ on the positive side. I have neglected the oscillating time dependence because of the steady-state assumption that the elastic displacement also oscillates with the same time dependence (at a different phase). In other words, the time dependence is not necessary because it cancels out.

References

[1] Chatterjee, Deep, *Design of a coating-less reference cavity with total internal reflection.* LIGO Report. (2013).

[2] Kessler et al. *A sub-40-mHz-linewidth laser based on a silicon single-crystal optical cavity.* Nature Photonics 6, 687692 (2012)

[3] Schiller, et al. *Fused-silica monolithic total-internal-reflection resonator.* Optics Letters (1991).

[4] Callen & Welton. *Irreversibility and Generalized Noise.* Physical Review 83, 34 (1951).

[5] Levin, Y. (1998). *Internal thermal noise in the LIGO test masses: A direct approach.* Physical Review D, 57(2), 659

[6] Landau & Lifshitz. *Theory of Elasticity.* Addison-Wesley, 1959. Page 18, eq. 7.4.

[7] Heinert, et al. *Thermorefractive noise of finite-sized cylindrical test masses.* Physical Review D84, 062001 (2011).

[8] Braginsky & Vyatchanin. *Corner reflectors and quantum-non-demolition measurements in gravitational wave antennae.* Physics Letters A. Volume 324, Issues 5-6, 26 April 2005, Pages 345-360.

[9] Liu & Thorne. *Thermoelastic noise and homogeneous thermal noise in finite sized gravitational-wave test masses.* Physical Review D62, 122002 (2000).